



OPEN

Two–three parameters isotherm modeling, kinetics with statistical validity, desorption and thermodynamic studies of adsorption of Cu(II) ions onto zerovalent iron nanoparticles

Adewumi O. Dada^{1,6,7}✉, Folahan A. Adekola², Ezekiel O. Odebunmi³, Adeniyi S. Ogunlaja⁴ & Olugbenga S. Bello^{1,5}

Adsorption of problematic copper ions as one of the endocrine disruptive substances from aqueous solution onto nanoscale zerovalent iron (nZVI) was studied. The high pore size 186.9268 Å, pore diameter 240.753 Å, and BET surface area 20.8643 m² g⁻¹ and pH(pzc) enlisted nZVI as an efficient nano-adsorbent for treatment of heavy metals from synthetic wastewater. SEM and EDX revealed the morphology and elemental distribution before and after adsorption. 98.31% removal efficiency was achieved at optimum adsorption operational parameters. Of all the thirteen isotherm models, equilibrium data were well fitted to Langmuir. Kinetics and mechanism data across the concentrations from 10 to 200 mg L⁻¹ were analyzed by ten models. PSO best described kinetics data as confirmed by various statistical error validity models. The intraparticle diffusion model described that the intraparticle diffusion was not the only rate-limiting step. The adsorption mechanism was diffusion governed established by Bangham and Boyd models. Feasible, spontaneous, endothermic, and degree of randomness were revealed by the thermodynamic studies. Better desorption index and efficiency were obtained using HCl suggesting multiple mechanism processes. The performance of ZVI suggested it has a great potential for effective removal of endocrine disruptive cationic contaminant from wastewater.

Endocrine disruptive compounds (EDC) have been among emerging contaminants whose adverse effects in the environments have received the attention of various researchers. Heavy metal ions have been identified to have hazardous effects on the endocrine system. Copper, as heavy metal ions, has been listed among endocrine disruptive compounds. Some of the endocrine disruptive effects of copper ions are: Increased levels of plasma cortisol associated with protein synthesis, cell proliferation, and apoptosis in gill cells. It can also lead to an increase in Catecholamines which promotes metabolic and haematopoietic responses^{1,2}. Several anthropogenic activities and natural phenomena release copper ions into the environment³. The largest threat to human lives and aquatic organisms arises from the soluble form of copper⁴. These soluble copper ions get released into the environment via different agricultural applications. Research has shown that high uptakes of copper may cause liver and kidney damage and even death⁵⁻⁷. Research on the utilization of nanoparticles is on the increase due to their special characteristics. Nanotechnology is a trending research area for the science and technology of

¹Nanotechnology Laboratory, Industrial Chemistry Programme, Department of Physical Sciences, Landmark University, P.M.B.1001, Omu-Aran, Kwara State, Nigeria. ²Department of Industrial Chemistry, University of Ilorin, P.M.B. 1515, Ilorin, Nigeria. ³Department of Chemistry, University of Ilorin, P.M.B. 1515, Ilorin, Nigeria. ⁴Department of Chemistry, Nelson Mandela Metropolitan University, P.O. Box 77000, Port Elizabeth 6031, South Africa. ⁵Department of Pure and Applied Chemistry, Ladoké Akintola University of Technology, P.M.B 4000, Ogbomosho, Oyo State, Nigeria. ⁶Landmark University, Sustainable Development Goal (SDG) Group 6: Clean Water and Sanitation, Omu-Aran, Nigeria. ⁷Landmark University, Sustainable Development Goal (SDG) Group 11: Sustainable Cities and Communities, Omu-Aran, Nigeria. ✉email: dada.oluwasogo@lmu.edu.ng

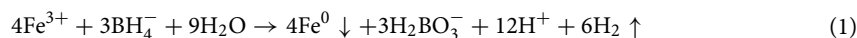
functional structures at the molecular scale. This covers current research work in chemical, physical, biological, medical, material sciences, and engineering. Nano-materials have been reported to be applicable in environmental remediation, catalysis, development of optical devices, and medicine⁸. Nanoparticles are the new trend of effective adsorbents used in the decontamination of water and immobilization of heavy metal ions from their solutions⁹. A study conducted by the U.S Environmental Protection Agency showed that zerovalent iron nanoparticle (nZVI) is environmentally benign and effective in soil and water remediation^{8,10–12}. nZVI has found relevance in the adsorption of problematic toxicants such as EDC heavy metal ions. Of all various conventional approaches¹³ described for heavy metal ions removal, adsorption via adsorption is much more favored since it is low cost, efficient, available, and easy to operation^{14–16}.

The most vital quantity for comprehending the adsorption process is gotten from adsorption isotherm models. The parameters of isotherm modeling are essential factors relevant to the design of an effluent treatment reactor. More so, extensive isotherm models were investigated to predict and compare adsorption performances. Most common isotherm models are Langmuir and Freundlich, Temkin and Dubinin–Kaganer–Raduskevich (DKR). Other isotherm models used in this study are Halsey, Jovanovic, Elovich, Jossen, Flory–Huggins, Kiselev, Harkins–Jura, Fowler–Guggenheim, and Redlich–Peterson. In most adsorption studies carried out using nZVI, no detailed investigation has been reported for mathematical isotherm parameters that could be utilized for treatment reactor design. This has not been given a priority hence a research gap of global interest has been created. The energy of the adsorption process for uptake of endocrine disruptive copper ions via thermodynamic studies was examined to determine the feasibility, spontaneity, energy content, and degree of disorderliness of the process. More so, the mechanism vis-à-vis desorption studies were investigated using three desorbing agents. The reality of the adsorption process was assessed by post-adsorption characterization using Fourier Transform Infrared Spectroscopy (FTIR), Scanning Electron Microscopy (SEM), and Energy Dispersive X-ray (EDX).

Materials and methods

All through this work, analytical grade reagents were used without further purification. Double-Distilled-Deionized water, Copper sulphate ($\text{CuSO}_4 \cdot 5\text{H}_2\text{O}$, Breckland Scientific Batch No. 6688), Isopropyl alcohol (BDH, Min. Assay 99%, Prd No. 29694 6). Other chemicals purchased from Sigma Aldrich, USA are Sodium borohydride (NaBH_4), Iron (III) chloride ($\text{FeCl}_3 \cdot 6\text{H}_2\text{O}$), Hydrochloric acid (HCl), Sodium hydroxide (NaOH), Sodium nitrate (NaNO_3).

Synthesis of zerovalent iron nanoparticles (nZVI). The synthesis of nZVI for the removal of endocrine disruptive heavy metal ions was undertaken by following the procedure described in our prior studies^{6,17}. Under an anaerobic environment, a resulting black coloration of core-shell zerovalent iron nanoparticles (nZVI) was obtained from the reaction between 0.023 M solution of $\text{FeCl}_3 \cdot 6\text{H}_2\text{O}$ and 0.125 M solution of NaBH_4 in ratio 1:5. Detailed synthetic procedure is presented in the supplementary document associated with this study. The synthesis equation is depicted in Eq. (1):



Surface charge (pH_{pzc}), BET surface area, surface morphology and elemental distribution. Following the salt addition and pH variation method, the point of zero charge was determined as presented in the supplementary materials¹⁸. Surface area by BET, pore width, and volume were determined using Micromeritics AutoChem II Chemisorption Analyzer. The surface morphological characterization and elemental analysis were carried out using a Scanning Electron Microscopy (SEM) integrated with Energy Dispersive X-ray (EDX) analyzer. SEM images and EDX spectra were obtained using a TESCAN Vega TS 5136LM typically at 20 kV at a working distance of 20 mm. Samples for SEM analysis were prepared by coating them in gold using a Balzers' Sputtering device.

Effect of stirring speed, pH, and co-existing ions. In order to optimize the stirring speed, 160–240 rpm speed was studied at optimum conditions. Effect of pH was studied by regulating the solution to the desired pH value using 0.1 M NaOH and 0.1 M HNO_3 solutions. Effect of Co-existing ions/Ionic strength varying the concentration of NaCl introduced into Cu^{2+} solution from 0.001 to 1.0 M.

Batch isotherm, kinetics, and thermodynamic studies. A typical batch adsorption study was carried out following procedure reported in our previous study^{19,20}. 1000 ppm Cu^{2+} stock solution was prepared by dissolving 2.5 g of $\text{CuSO}_4 \cdot 5\text{H}_2\text{O}$ in 1000 mL of distilled-deionized water. Study on initial Cu^{2+} ion concentration was examined by adding 100 mg nZVI at different Cu (II) ions concentrations (10–200 ppm) and residual concentration determined by using AAS model AA320N. The quantity adsorbed and percentage removal efficiency were calculated utilizing Eqs. (2) and (3)^{21–23}:

$$Q = \frac{(c_o - c_e)V}{m} \quad (2)$$

$$\% RE = \frac{C_i - C_e}{C_i} \times 100 \quad (3)$$

The characteristics and mechanism of the adsorption process were investigated from the study of the Ce-dependent changes of Q_e applied to thirteen isotherm models. Similarly, the batch adsorption kinetic experiments were conducted at optimum conditions for contact time ranging from 10 to 120 min. Adsorption capacities at contact time were obtained using Eq. (4)^{5,23}:

$$Q_t = \frac{(C_o - C_e)V}{W} \quad (4)$$

Kinetic data were fitted to ten kinetics and mechanism models.

From the thermodynamics studies, the effect of temperature at optimum conditions was investigated at five different temperatures (298 K, 303 K, 318 K, 328 K, 333 K) for adsorption of endocrine disruptive Cu^{2+} onto nZVI following our previously reported procedure^{24,25}. The study was carried out in a temperature-controlled water bath. Data obtained were fitted to Van't Hoff equation depicted in Eqs. (5) and (6).

$$\log K_C = \frac{\Delta S^\circ}{2.303R} - \frac{\Delta H^\circ}{2.303RT} \quad (5)$$

$$\Delta G = -2.303RT \log K_C \quad (6)$$

R is the gas constant ($8.314 \text{ J mol}^{-1} \text{ K}^{-1}$), T the absolute temperature (K), K_C (q_e/C_e) an equilibrium constant at various temperature. Standard enthalpy change ΔH° (kJ mol^{-1}) and standard entropy change ΔS° ($\text{J mol}^{-1} \text{ K}^{-1}$) were determined from the slope and intercept of the Van't Hoff plot of $\log K_C$ versus $1/T$ ^{26,27}.

Desorption studies. The desorption is a means of regenerating the adsorbent capacity for reusability and cost effectiveness determination. Desorption studies were investigated using the following eluents: deionized (DI) water, 0.2 M HCl and 0.2 M CH_3COOH , at pre-determined optimum conditions. The desorption capacity, percentage desorbed, desorption efficiency and desorption index were determined using Eqs. (7)–(10)²⁸:

$$q_{des} = C_{des} \frac{V}{W} \quad (7)$$

$$\% \text{ Desorption} = \frac{C_{des}}{C_i} \times 100 \quad (8)$$

$$\% \text{ Desorption Efficiency} = \frac{q_{des}}{q_e} \times 100 \quad (9)$$

$$\text{Desorption index} = \frac{\% \text{ total metal removed after adsorption}}{\% \text{ total metal remained on the adsorbent after desorption}} \quad (10)$$

where q_{des} is the quantity of metal ion desorbed (mg g^{-1}), q_e is the quantity of metal adsorbed after sorption (mg g^{-1}), C_{des} is the concentration of metal ion left after desorption (mg L^{-1}), V is the volume of the metal ion solution (mL) while W is the weight of adsorbents (mg).

Results and discussion

nZVI physicochemical characterization: pH(pzc), BET surface area, pore volume and pore size. Summarized in Table 1 are pH, point of zero charge (PZC), BET surface area, and other physicochemical parameters describing the core-shell. The point of zero charge finds relevance in surface and nanoscience.

Figure S1 (from the supplementary document associated with this study) shows the pH(pzc) of nZVI. It revealed that adsorption of Cu^{2+} would take place at a $\text{pH} > \text{pH}_{\text{pzc}}$ as a result of more active binding being available due to deprotonation and low electrostatic repulsion. This finding shows that nZVI was positive at $\text{pH} < \text{pH}_{\text{pzc}}$ and negative at $\text{pH} > \text{pH}_{\text{pzc}}$. Thus this signposts the suitability of nZVI for effective adsorption. The BET surface area $20.86 \text{ m}^2 \text{ g}^{-1}$ and the external surface area $16.4503 \text{ m}^2 \text{ g}^{-1}$ being greater than their corresponding micropores further support the suitability of nZVI for adsorption. Higher surface area enhances the adsorption process as supported. Therefore, it can be deduced that nZVI nano-adsorbent would utilize its external surfaces for heavy metal uptake than its micropore areas²⁹.

SEM/EDX characterization. Percolation of EDC- Cu^{2+} into the pores and matrix of nZVI was proved by the SEM/EDX depicted in Fig. 1A–D. Figure 1A revealed the SEM image before adsorption while Fig. 1B depicted the EDX with an intense peak of a zerovalent iron nanoparticle. Before adsorption spherical, chain-like aggregated morphology of nZVI was revealed SEM. The core-shell nature of zerovalent iron with intense peaks between 0.6–6.4 and 7.0 keV was revealed from the EDX result in Fig. 1B. Presented in Fig. 1C is the SEM micrograph showing swollen and robust nature of the surface of the nZVI nano-adsorbent after adsorption suggesting that the nZVI surface had been Cu-loaded up. More so, corroborating the result from SEM, Fig. 1D revealed the EDX spectrum showing the presence of Cu(II) as evidence of Cu adsorption onto core-shell nZVI. This is supported by finding in the literature³⁰.

Physicochemical parameters	nZVI
pH	6.80
PZC	5.84
BET surface area	20.8643 m ² g ⁻¹
t-Plot micropore area	4.4140 m ² g ⁻¹
t-plot external surface area	16.4503 m ² g ⁻¹
BJH adsorption cumulative surface area of pores	19.120 m ² g ⁻¹
Pore volume	
Single point adsorption total pore volume of pores	
less than 1103.482 Å diameter at P/Po = 0.982136052:	0.097502 cm ³ g ⁻¹
t-Plot micropore volume:	0.001895 cm ³ g ⁻¹
BJH adsorption cumulative volume of pores	0.115083 cm ³ g ⁻¹
Pore size	
Adsorption average pore width (4 V/A by BET):	186.9268 Å
BJH Adsorption average pore diameter (4 V/A):	240.753 Å

Table 1. Physicochemical parameters of nZVI.

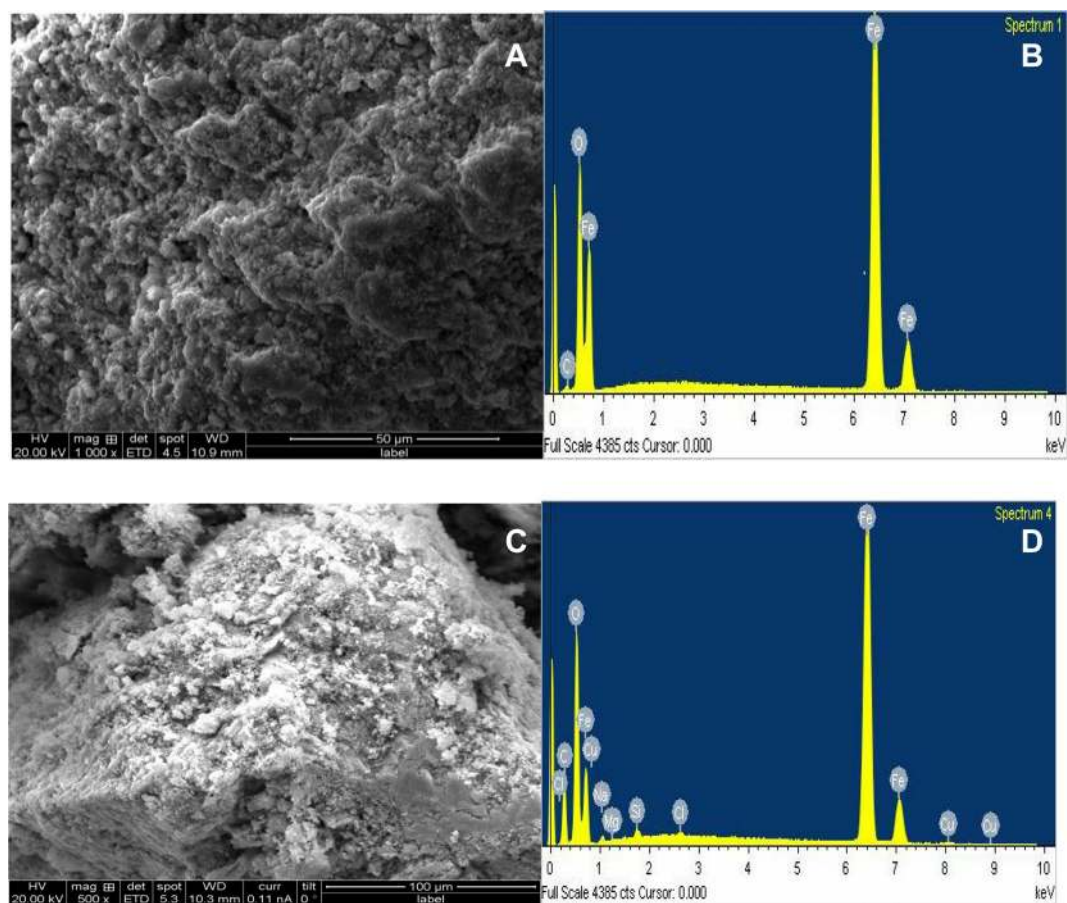


Figure 1. (A) SEM micrograph of nZVI before adsorption. (B) EDX spectrum of nZVI before adsorption. (C) SEM micrograph of Cu-loaded-nZVI after adsorption. (D) EDX of Cu-loaded-nZVI after adsorption.

Effect of operational parameters. *Effect of initial Cu²⁺ concentration.* A major role in the adsorption study is played by the factor of initial concentration at optimum conditions presented in supplementary document as seen in Figure S2 This showed that at optimum conditions, 85.04% RE and 81.04 mgg⁻¹ quantity of Cu²⁺ was adsorbed. The extent of removal of Cu(II) ion cation increased based on the availability of more active sites at lower concentrations until the pore sizes were saturated at an advanced concentration (150–200 mg L⁻¹).

Concentration gradient was built up in the Cu-nZVI system due to intensification of drive force as concentration increased from 10 to 200 mg L⁻¹. This is supported by the findings in the literature³¹.

Effect of contact time. The Build-up of Cu(II) ions at the solid–liquid interfaces are controlled by the contact time. From this study, optimization of the contact time was investigated from 10 to 120 min. Fast kinetics from the bulk to the outer and inner surface of the nano-material (nZVI) identified by a short contact time to reach equilibrium was observed in the supplementary document as seen in Figure S3 Quantity of Cu(II) adsorbed increase from 4.96 to 82.82 mg g⁻¹ as the initial Cu²⁺ concentration increased from 10 to 200 ppm. A similar trend was observed by Baby et al.³² on the adsorption of heavy metals.

Effect of initial solution pH. The key to the adsorption of heavy metal ions is the solution pH because it affects the surface chemistry of the system. A plot of the effect of initial concentration is presented in the supplementary document as seen in Figure S4 portrayed the effect of pH at optimum conditions. Coined from the understanding of the isoelectric point of the pH(pzc), nZVI is suitable for the uptake of cationic pollutants such as Cu²⁺ since the pH > pH(pzc). At low solution pH, the system is protonated leading to electrostatic competition among Cu²⁺ and other cationic species such as H⁺, Cu(OH)⁺, Cu(OH)₂. However, at solution pH > pH(pzc), the system is negative, deprotonation occurs, there is less competition between Cu²⁺ and other anionic species (Cu(OH)₃⁻ and Cu(OH)₄²⁻). Effective adsorption occurs at pH > pH(pzc). Optimum adsorption was achieved at pH 6 with 98.31% removal efficiency and quantity adsorbed 73.73 mg g⁻¹ indicating effective binding of Cu²⁺ onto nZVI surface. This is corroborated by the findings of other researchers³³.

Effect of ionic strength. Analysis of Figure S5 (presented in the supplementary document associated with this study) showed the effect of ionic strength on Cu²⁺ adsorption. Pollution of the water system is not limited to heavy metal ions only, some co-existing ions increase the salinity and ionic strength of the water body as investigated in this study. Co-existing ions polluted waste system increases the salinity and background electrolyte of the water body. A decrease in the percentage of Cu²⁺ removed from 81.99 to 79.73% with a reduction in quantity adsorbed from 61.49 to 59.79 mg g⁻¹ was observed in Figure S5. The decrease in Cu(II) ions uptake may also be due to a decrease in the electrostatic attraction arising from compressed electrical diffuse double layer supporting the findings of Advantageously, the removal efficiency of 81.99% shows that nZVI is an effective nano-sorbent in treatment industrial discharge containing co-existing ions. This is supported by findings in the literature³⁴.

Effect of stirring speed. This study demonstrated as shown in Figure S6 (supplementary document) that at 200 rpm maximum adsorption of Cu²⁺ onto nZVI was attained. Stirring speed is also one of the important parameters in adsorption studies because it promotes turbulence, frequency of collision and improves mass transfer in the medium between the two phases. At 200 rpm, the percentage Cu²⁺ removal efficiency and quantities adsorbed are 96.98% and 72.73 mg g⁻¹ for nZVI. Stirring speed increases the retention of Cu²⁺ and it encourages a better transfer of Cu²⁺ between solid–liquid interfaces (Cu²⁺-nZVI system)¹⁸. No appreciable percentage removal efficiency was observed after 200 rpm and all other study was carried out at this stirring speed.

Two–three parameters adsorption isotherm modelings. One of the important and significant aspects of adsorption studies is mathematical isotherm modeling. Isotherm modeling is important in order to observe the relationship between nZVI and Endocrine disruptive Cu(II) ions at equilibrium conditions. A good understanding of this would significantly enhance the design of the adsorption system, effluent treatment reactor, and the pattern describing adsorbate-adsorbent interaction. Equilibrium data obtained from initial concentration were analyzed using thirteen mathematical isotherm models. All mathematical isotherm models used in this study were presented in Table 2 together with their non-linear, linear equations and parameters' description. The estimated parameters are portrayed in Table 3. The plots in the isotherm studies are presented in the supplementary document associated with this article from Figure S7A–S7M.

Langmuir isotherm model (Figure S7A) assumes no interaction of the neighboring sites, monolayer surface, identical active sites, uniformity in adsorption energy¹⁴. The non-linear and linear Langmuir equations are presented in Eq. (11). In this study, the Langmuir isotherm model has the highest correlation coefficient (R² > 0.97) indicating the appropriateness and best fitting of equilibrium data to the Langmuir model. The Langmuir essential feature, as well as the separation factor or dimensionless constant (R_L), was calculated using Eq. (12)²⁰. Values of calculated characteristics parameters are presented in Table 3. The values of R_L (1 > R_L > 0) portrayed in Table 3 supported favorable adsorption process³⁵.

Freundlich isotherm model is presented in Eq. (13) (Table 2) and the plot is as depicted in Figure S7B. The characteristic parameters are represented in Table 3. The values 12.54 and 1.83 indicated Freundlich capacity (K_F) and intensity (n_F) of adsorption respectively. The values of n_F also measure whether the adsorption is favorable or not. The value of 1/n_F (0.5457) less than unity and n_F greater than unity and less than 10 indicated a normal and favorable adsorption^{36,37}. Temkin model (Eq. 14) fits the experimental data (R² = 0.95) as depicted in Figure S7C. The positive value of B (14.678) and high b_T (168.794 J mol⁻¹) revealed the binding of Cu²⁺ onto nZVI as well as the endothermic nature of the system. A report from other researchers corroborated this³⁶.

Equations (15)–(17) defined the Dubinin–Kaganer–Raduskevich (DKR) model, Polanyi potential, and adsorption free energy of DRK. DRK plot is presented in Figure S7D and Table 3 shows evaluated parameters. The DKR free energy (E = 1581.14 J mol⁻¹) lower than 8 kJ mol⁻¹ supported that electrostatic interaction between Cu²⁺-nZVI system is Physisorption mechanism³⁸. Halsey isotherm model (Eq. 18 and plot in Figure S7E) with parameters of K_H and n_H (0.0097 and -1.8325) further supported normal and favorable adsorption indicated by

Types of adsorption models	Non-linear expression	Linear expression	Parameters nomenclature and description
Langmuir	$Q_e = \frac{Q_{max}K_L C_e}{1+K_L C_e}$	$\frac{C_e}{Q_e} = \frac{C_e}{Q_{max}} + \frac{1}{Q_{max}K_L}$ (11) $R_L = \frac{1}{1+K_L C_e}$ (12)	K_L is the Langmuir isotherm constant ($L\ mg^{-1}$) related to the binding energy of adsorption. Q_{max} is the maximum monolayer coverage capacity ($mg\ g^{-1}$) R_L dimensionless separation factor indicating the nature and favourability of adsorption process. From slope and intercept of linear plot of C_e/Q_e versus C_e , K_L and Q_{max} were determined
Freundlich	$Q_e = K_F C_e$	$\log Q_e = \log K_F + \frac{1}{n_F} \log C_e$ (13)	C_e equilibrium concentration of the MG dye adsorbate ($mg\ L^{-1}$); Q_e amount of MG dye adsorbed at equilibrium per unit weight of nZVI ($mg\ g^{-1}$); K_F Freundlich indicator of adsorption capacity $1/n_F$ Intensity of the adsorption indicating the surface heterogeneity and favourability of the adsorption process. $1/n_F$ and K_F were determined from slope and intercept of linear plot of $\log Q_e$ versus $\log C_e$
Temkin	$Q_e = \frac{RT}{b_T} \ln(A_T C_e)$	$Q_e = \frac{RT}{b_T} \ln A_T + \frac{RT}{b_T} \ln C_e$ (14)	b_T is the Temkin isotherm constant related to the heat of adsorption and A_T is the Temkin isotherm equilibrium binding constant ($L\ g^{-1}$) R = universal gas constant ($8.314\ J\ mol^{-1}\ K^{-1}$) T = absolute Temperature in Kelvin $B = RT/b_T$ = constant related to heat of sorption ($J\ mol^{-1}$) obtained either from intercept or slope
DKR	$Q_e = Q_{DKR} \exp^{-A_{D-R} \varepsilon^2}$	$\ln q_e = \ln Q_{DKR} - A_{DKR} \varepsilon^2$ (15) $\varepsilon = RT \ln \left[1 + \frac{1}{C_e} \right]$ (16) $E = - \left[\frac{1}{\sqrt{2A_{D-R}}} \right]$ (17)	Q_{DKR} is the theoretical adsorption isotherm saturation capacity ($mg\ g^{-1}$) obtained from intercept. $A_{D,R}$ is the D-R isotherm constant ($mol^2\ kJ^{-2}$) related to free sorption energy obtained from the slope. ε is Polanyi potential determined by the expression = $RT \ln(1 + 1/C_e)$. E is the mean adsorption free energy helpful in determining the adsorption nature (physisorption or chemisorption of the adsorption process). $Q_{D,R}$ and $A_{D,R}$ were determined from intercept and slope of linear plot of $\ln q_e$ versus ε^2
Halsey	$Q_e = \exp \left[\frac{\ln K_H - \ln C_e}{n_H} \right]$	$\log Q_e = \left[\left(\frac{1}{n_H} \right) \ln K_H \right] - \left(\frac{1}{n_H} \right) \ln C_e$ (18)	K_H is Halsey isotherm constant; n_H is the Halsey isotherm exponent. Both were determined from linear plot of $\log Q_e$ versus $\ln C_e$
Harkin-Jura	$Q_e = \left(\frac{A_{HJ}}{B_{HJ} - \log C_e} \right)^{\frac{1}{2}}$	$\frac{1}{Q_e^2} = \frac{B_{HJ}}{A_{HJ}} - \frac{1}{A_{HJ}} \log C_e$ (19)	A_{HJ} is the Harkins-Jura isotherm parameter B_{HJ} is the Harkins-Jura isotherm constant The Harkin-Jura constants, A_{HJ} and B_{HJ} , were determined from the slope and intercept of the linear plot of $1/Q_e^2$ versus $\log C_e$
Redlich-Peterson	$Q_e = \frac{A_{R-P} C_e}{1 + B_{R-P} C_e^\beta}$	$\ln \left(\frac{C_e}{Q_e} \right) = \beta \ln C_e - \ln A_{R-P}$ (20)	A_{R-P} is the Redlich-Peterson model isotherm constant ($L\ g^{-1}$). B_{R-P} is the Redlich-Peterson model constant ($mg\ L^{-1}$); β is the Redlich-Peterson model exponent, should be $0 \leq \beta \leq 1$. Parameters were determined from the plot of $\ln(C_e/Q_e)$ versus $\ln C_e$
Jovanovic	$Q_e = Q_J [1 - \exp(-K_J C_e)]$	$\ln Q_e = \ln Q_{max} - K_J C_e$ (21)	K_J is Jovanovic isotherm constant ($L\ g^{-1}$) determined from the slope of plot of $\ln q_e$ against C_e
Elovich	$\frac{Q_e}{Q_{max}} = K_E C_e \exp \frac{Q_e}{Q_{max}}$	$\ln \left(\frac{Q_e}{C_e} \right) = \ln K_E Q_{max} - \frac{Q_e}{Q_{max}}$ (22)	K_E is Elovich equilibrium constant ($L\ mg^{-1}$) Q_{max} is Elovich maximum adsorption capacity ($mg\ g^{-1}$). Elovich constants were determined from slope and intercept of the linear plot of $\ln \left(\frac{q_e}{C_e} \right)$ vs q_e
Jossen	$C_e = \frac{Q_e}{H} \exp \left(F q_e^p \right)$	$\ln \left(\frac{C_e}{Q_e} \right) = -\ln H + F q_e^p$ (23)	H is Jossens isotherm constant (it corresponds to Henry's constant), p is Jossens isotherm constant and it is characteristic of the adsorbent irrespective of temperature and the nature of adsorbents, and F is Jossens isotherm constant. H and F depend only on temperature Jossen's constants were determined from the linear plot of $\ln \left(\frac{C_e}{q_e} \right)$ vs q_e
Kiselev	$k_1 C_e = \frac{\theta}{(1-\theta)(1+k_n \theta)}$	$\frac{1}{C_e(1-\theta)} = \frac{K_1}{\theta} + K_1 K_n$ (24)	K_1 is Kiselev equilibrium constant (Lmg^{-1}) and K_n is equilibrium Constant of the formation of complex between adsorbed molecules. Kiselev constants were determined from the plot of $1/C_e(1 - \theta)$ versus $1/\theta$
Flory-Huggins	$\frac{\theta}{C_e} = K_{FH} (1 - \theta)^{n_{FH}}$	$\log \left(\frac{\theta}{C_e} \right) = \log K_{FH} + n_{FH} \log(1 - \theta)$ (25) $\theta = 1 - \left(\frac{C_e}{C_0} \right)$ (26)	θ is degree of surface coverage, n_{FH} is number of adsorbates occupying adsorption sites, and K_{FH} is Flory-Huggins equilibrium constant ($L\ mol^{-1}$). n_{FH} and K_{FH} were determined from the linear plot of $\log(\theta/C_e)$ versus $\log(1 - \theta)$
Fowler-Guggenheim	$K_{FG} C_e = \frac{\theta}{1-\theta} \exp \left(\frac{2\theta W}{RT} \right)$	$\ln \left[\frac{C_e(1-\theta)}{\theta} \right] = -\ln K_{FG} + \frac{2\theta W}{RT}$ (27)	K_{FG} is the Fowler-Guggenheim (F-G) equilibrium constant ($L\ mg^{-1}$), θ the fractional coverage, R the universal gas constant ($kJ\ mol^{-1}\ K^{-1}$), T the temperature (K), and W is the interaction energy between adsorbed molecules ($kJ\ mol^{-1}$). K_{FG} and W were determined from the linear plot of $\ln \left[\frac{C_e(1-\theta)}{\theta} \right]$ versus θ

Table 2. Adsorption isotherm and kinetics models^{35,43,47}.

the Freundlich isotherm model. However, the negative value of n_H couple with the low R^2 value of Harkin-Jura (Eq. 19, Figure S7F) showed that the adsorption nature of the nZVI surface is not multilayer and heterogeneous³⁹.

Combination of both the Langmuir and Freundlich isotherm attribute could be assessed in Redlich-Peterson Isotherm model (Eq. 20, Figure S7G). Redlich-Peterson correlation value ($R^2 = 0.9475$) shows its versatility and fitting to equilibrium data^{40,41}. Figure S7H depicts the Jovanovic isotherm (Eq. 21) model plot. Elovich isotherm model (Eq. 22, Figure S7I) has a foundation on the kinetic principle with the assumption of an increase in the adsorption sites exponentially⁴². It also takes into consideration the maximum monolayer capacity (Q_{max}). Based on R^2 value, the equilibrium data were fitted to the Elovich model but it was not as better described as compared to the Langmuir model. Also, its estimated $Q_{max} = 32.573\ mg\ g^{-1}$ (Table 3) being less than that of Langmuir signposted Langmuir as a better model. Jossen's isotherm model (Eq. 23, Figure S7J) is based on a distribution of the energy of interactions between the system solid-liquid system⁴³. Jossen's fit equilibrium data with $R^2 > 0.97$ (Table 3). Both Kiselev Isotherm Model (Eq. 24, Figure S7K) and the Flory-Huggins isotherm model (Eq. 25, Figure S7L) take into consideration the surface coverage (θ) of the Cu^{2+} adsorbate on the nZVI. Jovanovic isotherm model corresponds to another approximation for monolayer localized adsorption without

Langmuir	Parameters	Freundlich	Parameters	Temkin	Parameters	DKR	Parameters	Halsey	Parameters
Q_{\max} (mg g ⁻¹)	90.0901	k_f	12.5401	A_T	3.828	Q_d	51.9873	$1/n_H$	- 0.5457
K_L (L mg ⁻¹)	0.1563	$1/n_f$	0.5457	B (L g ⁻¹)	14.678	A_{DKR}	$- 2 \times 10^{-7}$	n_H	- 1.8325
R_L	0.3591	n_f	1.8325	b_T (J mol ⁻¹)	168.7949	E	1581.14	K_H	0.0097
R^2	0.9752	R^2	0.963	R^2	0.9586	R^2	0.8847	R^2	0.963
Harkin–Jura	Parameters	Redlich–Peterson	Parameters	Jovanovic	Parameters	Elovich	Parameters	Jossen	Parameters
$1/A_{H-J}$	0.0177	A_{R-P}	4.69×10^{-3}	Q_{\max}	13.8668	Q_{\max}	32.573	F	0.0307
A_{HJ}	56.4972	B (L g ⁻¹)	2.085	K_J	- 0.0556	K_E	1.1007	H	1.0312
B_{HJ}	1.2203	b	5.21×10^{-5}						
R^2	0.7025	R^2	0.9475	R^2	0.6105	R^2	0.9714	R^2	0.9714
Kiselev	Parameters	Flory–Huggins	Parameters	Fowler–Guggenheim	Parameters				
K_i	2852.4	n_H	- 1.3651	K_{FG}	2.6963				
K_n	0.6052	K_H	0.0329	W	881.02				
R^2	0.7566	R^2	0.8803	R^2	0.9487				

Table 3. Isotherm models and their various evaluated parameters for the adsorption of Cu²⁺ onto nZVI.

S. no.	Adsorbents	Adsorption capacity (Q_{\max}) (mg/g)	References
1	Pectin-iron oxide	48.99	10
2	Chitosan-bound Fe ₃ O ₄ magnetic nanoparticles	21.5	41
3	Aminated polyacrylonitrile nanofiber mats	30.40	29
4	Carbon nanotubes	24.49	42
5	Carboxymethyl- β -cyclodextrinconjugated magnetics nanoparticle	47.29	43
6	Fe ₃ O ₄ magnetic nanoparticles coated with humic acid	46.3	44
7	Magnetic gamma-Fe ₂ O ₃ nanoparticles coated with poly-L-cysteine	42.9	45
8	Magnetic nano-adsorbent modified by gum arabic	38.5	46
9	Hydroxyapatite nanoparticles	36.9	47
10	Maghemite nanoparticle	27.7	48
11	Amino-functionalized magnetic nanosorbent	25.77	49
12	Poly(hydroxyethyl methacrylate)	58.0	50
13	Fe ₃ O ₄ nanoparticle	37.04	51
14	Fe ₂ O ₃ nanoparticle	19.61	51
15	nZVI	90.09	This present study

Table 4. Comparison of adsorption capacity nZVI if other nano-adsorbents used for Cu²⁺ removal.

lateral interactions which ought to be similar to the Langmuir isotherm model. However, a lower correlation coefficient ($R^2 = 0.6105$) obtained in this study indicated that there is a lateral interaction and thus this model lower approach towards saturated compared to Langmuir adsorption isotherm as reported by Al-Ghouti et al.⁴⁴. This is supported by the fit and parameters obtained from Fowler–Guggenheim (F–G) isotherm model (Eq. 27, Figure S7M). Taken into consideration is the lateral interaction of adsorption of EDC–Cu²⁺ onto nZVI by the FG- isotherm model⁴⁵. As reported by the literature, the interaction between the adsorbed molecule is attractive, if W is positive; repulsive interaction if W is negative and no interaction between the adsorbed molecules will be observed if $W = 0$ ^{42,46}. In this study, the fit of the Fowler–Guggenheim isotherm model ($R^2 = 0.9487$) and positive value of W ($W = 881.02$ J mol⁻¹) indicated that there is positive contact in the Cu²⁺–nZVI system, hence the adsorption heat increased with loading confirming endothermic adsorption process as observed in the thermodynamics studies.

The screening and arrangement are based on the understanding of the important parameters (Q_{\max} and R^2). With regards to Q_{\max} (in descending order) Langmuir > DKR > Elovich > Jovanovic. With respect to R^2 (in descending order): Langmuir > Jossen = Elovich > Freundlich = Halsey > Temkin > Fowler–Guggenheim > DKR > Flory–Huggins Kiselev > Harkin–Jura > Jovanovic. Presented in Table 4 is the comparison of maximum monolayer adsorption capacities of adsorption of Cu²⁺ onto various nano-adsorbents and nZVI used in this study. It is obvious that nZVI exceedingly surpassed other existing adsorbents reported. This indicated that nZVI is an excellent potential nano-adsorbent for effective removal of endocrine disruptive heavy metal ions.

Adsorption kinetic with statistical error validity modeling. A kinetic study was undertaken to understand the controlling pathway, the rate of surface adsorption of the contaminant to the adsorbent, and the

quantity of the adsorption capacity. The kinetics equations vis-à-vis pseudo-first-order (PFO), pseudo-second-order (PSO), Elovich, Avrami, and Power Function (Fractional power) are represented on Eqs. (28)–(34)⁴⁷.

$$\text{Pseudo first-order (Lagergren's rate equation)} \quad \log(q_e - q_t) = \log q_e - \frac{k_1 t}{2.303} \quad (28)$$

$$h_1 \text{ initial pseudo first-order adsorption rate (mg g}^{-1} \text{ min}^{-1}) \quad h_1 = k_1 q_e \quad (29)$$

$$\text{Pseudo second-order rate equation:} \quad \frac{t}{q_t} = \frac{1}{k_2 q_e^2} + \frac{1}{q_e} t \quad (30)$$

$$h_2 \text{ is the initial pseudo second-order adsorption rate:} \quad h_2 = k_2 q_e^2 \quad (31)$$

$$\text{Elovich model:} \quad q_t = \frac{1}{\beta} \ln(\alpha\beta) + \frac{1}{\beta} \ln(t) \quad (32)$$

$$\text{Avrami model:} \quad \ln \left(\ln \left(\frac{q_e}{q_e - q_t} \right) \right) = n \ln k_{Av} + n \ln t \quad (33)$$

$$\text{Power Function:} \quad \log(q_t) = \log(k) + v \log(t) \quad (34)$$

The kinetic plots are presented in Fig. 2A–E with error bars indicating the application of error models and the evaluated parameters are presented in Table 5. The kinetic constant k_1 of Pseudo first order (PFO), its adsorption rate constant h_1 , disagreement between $q_{e, \text{exp}}$ and $q_{e, \text{cal}}$ and low correlation coefficient, $R^2 < 0.90$, demonstrated that PFO is not applicable in this study. A similar low trend in the R^2 value was observed in the Avrami model demonstrating that it is not applicable in this study. A good agreement between the experimental quantity adsorbed ($q_{e, \text{exp}}$) and the calculated quantity adsorbed ($q_{e, \text{cal}}$) was observed in PSO, Elovich, and Power function. From the Elovich model, the values of α (adsorption rate) increased with an increase in concentration as a result of an increase in the number of sites. The values of $1/\beta$ at 10 ppm, 50 ppm, 100 ppm, and 150 ppm are 5.882, 11.764, and 17.123 respectively. These values reflect the number of sites available for adsorption³⁰. Kinetic parameters from Power Function in Table 5 indicated time-dependent of Cu(II) onto nZVI with the value of constant v less than 1 across all the concentrations. Of all these kinetic models, PSO best described the Cu(II) adsorption process and this was supported by the statistical error validity model presented in Table 5. The PSO initial adsorption rate (h_2) increases with increase in concentration from 33.67 to 238.095 $\text{mg g}^{-1} \text{ min}^{-1}$. R^2 values range from 0.99 to unity demonstrating the best fitting by PSO suggesting chemisorption mechanism.

Statistical validity of the kinetic models. Assessment on the best kinetic fitting model that is always based on linear regression coefficient could be biased inherent, hence the need for statistical validity model. The suitability, agreement, and best fit among the kinetic models are judged not only by regression coefficient (R^2) but also with the use of statistical error validity models. Validity of kinetic data was fitted to statistical error models namely; Average relative error (ARE), Normalized Standard Deviation Δq (%), Hybrid fractional error function (HYBRD), Derivative of Marquardt's percent standard deviation (MPSD), Standard deviation of relative Error (S_{RE}). The various statistical functions are presented in Table 6. Presented in Table 7 are the statistical error validity data of the kinetic models. Five statistical tools were used for the validity of these kinetic models. It is observed that the closer the agreement between the experimental quantity adsorbed (q_e, exp) and calculated quantity adsorbed (q_e, cal), the lower the values of these statistical tools, the better the model. In order to justify and juxtapose the best model, a reference was made to the coefficient of regression (R^2). The higher the R^2 values, the closer the values of q_e, exp , and q_e, cal , the lower the values of Δq , HYBRID, MPSD, ARE, and S_{RE} , the better the kinetic models in describing the sorption process^{48–50}. The values in Table 4 vividly show that pseudo-second-order at various initial Cu^{2+} concentrations (10 ppm, 50 ppm, 100 ppm, 150 ppm, and 200 ppm) best describe the sorption process. the model can be arranged in descending order with respect to R^2 : pseudo-second-order > Elovich > fractional power > Avrami > pseudo-first-order.

Adsorption mechanisms for sorption of Cu^{2+} onto nanoscaled zerovalent iron (nZVI). Figure 3A–E show the linear plots of intraparticle diffusion, liquid diffusion, external diffusion, Bangham and Boyd models. Adequate understanding of the adsorption mechanism is enhanced by the determination of the rate-controlling/determining step. The three definite steps that could be used to describe the adsorption rate are⁵¹: (1) Intraparticle or pore diffusion, where adsorbate molecules percolate into the interior of adsorbent particles, (2) Liquid film or surface diffusion where the adsorbate is transported from the bulk solution to the external surface of the adsorbent, and (3) adsorption on the interior sites of the sorbent. Since the plot of Intraparticle diffusion (Fig. 3A) did not pass through the origin, it is demonstrated that it is not the only rate-determining step⁵². Other mechanisms such as surface diffusion and external diffusion also participated in the mechanism of Cu(II) removal. However, the higher R^2 values of intraparticle diffusion from the evaluated parameters presented in Table 8 demonstrated that the mechanism is pore diffusion dependent which was confirmed by Bangham and scattered plot of Boyd models^{53,54}. The intercept of intraparticle diffusion which is the thickness of the

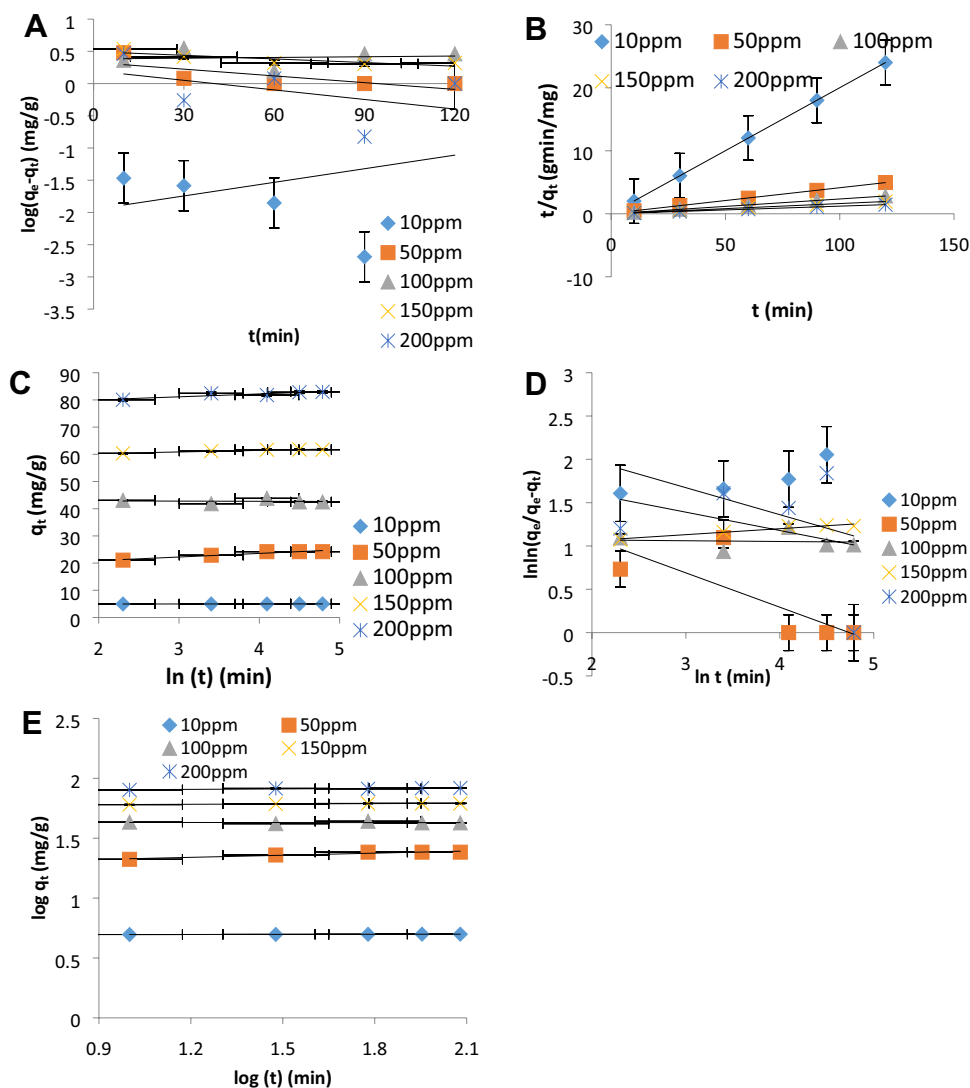


Figure 2. (A–E): Linearized plots of (A) pseudo-first-order rate equation, (B) pseudo-second-order rate equation, (C) Elovich rate equation, (D) Avrami kinetics models, (E) fractional power rate equation models for adsorption of Cu^{2+} onto nZVI at 10 ppm, 50 ppm, 100 ppm, 150 ppm and 200 ppm.

surface gives information about the contribution of the surface sorption in the rate-determining step. The larger the intercept, the greater the contribution of nZVI in adsorption of Cu^{2+} as observed from the trend across the concentrations investigated.

Thermodynamics analysis. Thermodynamics analysis is imperative to determine the (enthalpy change) heat content (ΔH); entropy change (degree of randomness, ΔS), possibility, and spontaneity (Gibbs free energy change, ΔG) in every adsorption process. The plots in thermodynamics studies are presented in the supplementary document associated with this article. As observed in Figure S8, intensification in the percentage removal efficiency was attained with an increase in temperature of the system supporting the endothermic process. This is due to a decrease in the mass transfer resistance and boundary layer thickness of nZVI⁵⁵. Van't Hoff's linear plot of $\log K_c$ against $1/T$ was portrayed in Figure S9 and the result obtained was presented in Table 9. The positive value of ΔH ($+50.6059 \text{ kJ mol}^{-1}$) confirmed that the adsorption process is endothermic in nature⁵⁶. The positive value of ΔS ($+174.679 \text{ J mol}^{-1} \text{ K}^{-1}$) shows an increase in the degree of randomness of the lateral interaction during the adsorption of Cu^{2+} at the solid/liquid interface. This could be enhanced by the appropriate stirring speed. The feasibility and spontaneity of the adsorption process are confirmed by the negative values of ΔG (-1.6765 to $7.9602 \text{ kJ mol}^{-1}$).

Desorption mechanism. Figure 4 shows the comparative effect of different eluents in the desorption of Cu^{2+} from Cu^{2+} -loaded nZVI. The opportunity to investigate regeneration and reusability of loaded adsorbent is enhanced by desorption studies. The effectiveness of three different eluents and desorbing agents (HCl, CH_3COOH , and H_2O) was investigated. The basic desorption mechanisms are ion exchange, complexation, and

Kinetics model parameters	Initial Cu ²⁺ concentration					
	Evaluated parameters	10 ppm	50 ppm	100 ppm	150 ppm	200 ppm
PFO						
	q _e , exp (mg g ⁻¹)	4.9859	24.1981	43.8152	61.684	81.77
	q _e , cal (mg g ⁻¹)	0.01109	2.1311	2.3147	3.1261	1.5816
	k ₁ (min ⁻¹)	- 0.0161	8.065 × 10 ⁻³	- 9.212 × 10 ⁻⁴	4.375 × 10 ⁻³	1.152 × 10 ⁻²
	h ₁ (mg g ⁻¹ min ⁻¹)	1.785 × 10 ⁻⁴	1.717 × 10 ⁻²	2.22 × 10 ⁻³	1.367 × 10 ⁻²	1.822 × 10 ⁻²
	R ²	0.1029	0.5549	0.0147	0.7275	0.2127
PSO						
	q _e , exp (mg g ⁻¹)	4.9859	24.1981	43.8152	61.684	81.77
	q _e , cal (mg g ⁻¹)	5.005	24.6305	42.5532	61.728	83.333
	k ₂ (g mg ⁻¹ min ⁻¹)	1.3441	0.02813	3.7301	3.8572	2
	h ₂ (mg g ⁻¹ min ⁻¹)	33.67	17.0648	158.73	238.095	166.667
	R ²	1	0.9999	0.9999	1	0.9999
Elovich						
	q _e , exp (mg g ⁻¹)	4.9859	24.1981	43.8152	61.684	81.77
	q _e , cal (mg g ⁻¹)	4.9889	23.6859	42.7181	61.4962	82.3027
	α (g min ² mg ⁻¹)	6.449 × 10 ⁺¹⁴⁵	1.289 × 10 ⁺⁶	- 4.39 × 10 ⁻²⁸³	1.3162 × 10 ⁺⁴⁴	7.4216 × 10 ⁺³¹
	β (g min mg ⁻¹)	68.9655	0.755	- 15.0602	1.7274	0.9406
	R ²	0.9397	0.9336	0.0078	0.9357	0.7967
Avrami						
	q _e , exp (mg g ⁻¹)	4.9859	24.1981	43.8152	61.684	81.77
	q _e , cal (mg g ⁻¹)	4.873	17.5472	41.307	60.1006	78.3886
	n _{av}	- 0.3116	- 0.3962	- 0.0086	0.068	- 0.2113
	K _{av}	2.3201	8.74 × 10 ⁻³	1.4047	6.977 × 10 ⁺⁵	6.9246
	R ²	0.1457	0.5795	0.0065	0.9414	0.0852
Fractional power						
	q _e , exp (mg g ⁻¹)	4.9859	24.1981	43.8152	61.684	81.77
	q _e , cal (mg g ⁻¹)	4.9906	23.6629	42.7202	61.5025	82.2843
	v (min ⁻¹)	2.9 × 10 ⁻³	5.83 × 10 ⁻²	- 1.5 × 10 ⁻³	9.5 × 10 ⁻³	1.3 × 10 ⁻²
	k ₃ (mg g ⁻¹)	4.9295	18.638	42.9833	59.1561	78.0189
	k ₃ v (mg g ⁻¹ min ⁻¹)	1.429 × 10 ⁻²	1.0866	6.447 × 10 ⁻²	5.619 × 10 ⁻¹	1.0142
	R ²	0.94	0.9311	0.0078	0.9352	0.7967

Table 5. Kinetic data for adsorption of Cu²⁺ onto nZVI at different initial concentrations.

Normalized standard deviation Δq _t (%)	$\Delta q(\%) = 100 \sqrt{\frac{\sum_{i=1}^n \left(\frac{q_{e,exp} - q_{e,cal}}{q_{e,exp}} \right)^2}{n-1}}$	15
Hybrid fractional error function (HYBRID)	$HYBRID = \sum_{i=1}^n \left[\frac{(q_{e,exp} - q_{e,cal})^2}{q_{e,exp}} \right]_i$	16
Derivative of Marquardt's percent standard deviation (MPSD)	$MPSD = \sum_{i=1}^n \left[\frac{(q_{e,exp} - q_{e,cal})^2}{q_{e,exp}} \right]^2$	17
Average relative error (ARE)	$ARE = \sum_{i=1}^n \left[\frac{q_{e,exp} - q_{e,cal}}{q_{e,exp}} \right]$	21
Standard deviation of relative errors (S _{RE})	$S_{RE} = \sqrt{\frac{\sum_{i=1}^n [(q_{e,exp} - q_{e,cal}) - ARE]^2}{n-1}}$	22

Table 6. Adsorption statistical error validity models (ASEVM)^{24,43,44,46}.

precipitation depending on the most effective desorbing agent⁵⁷. The exact mechanism involved in the adsorption process is revealed by the performance of the most effective desorbing agent. The maximum percentage of Cu(II) desorbed from Cu(II) loaded-nZVI using HCl was 79.89% showing the best desorption index of 3.39. The effectiveness of HCl as the best desorbing agent among the three eluents used is supported by the findings of Reddiar et al. (2019)⁵⁰ Acetic acid also performed averagely while distilled-deionized water was a poor desorbing agent in the desorption of Cu(II) from Cu(II)-loaded-nZVI. Thus, the adsorption of Cu(II) onto nZVI

Adsorption statistical error validity models on kinetics of adsorption	Data at various initial Cu ²⁺ concentrations				
	10 ppm	50 ppm	100 ppm	150 ppm	200 ppm
Pseudo first-order					
q _e ,exp (mg g ⁻¹)	4.9859	24.1981	43.8152	61.684	81.77
q _e , cal (mg g ⁻¹)	0.01109	2.1311	2.3147	3.1261	1.5816
R ²	0.1029	0.5549	0.0147	0.7275	0.2127
HYBRID	4.9637	20.1236	39.3081	55.5902	78.6374
MPSD	0.9956	0.8316	0.8971	0.9012	0.9617
ARE	0.9978	0.9119	0.9472	0.9493	0.9806
Δq	24.9444	22.7983	23.6792	23.7330	24.5165
S _{RE}	1.98852	10.5775	20.2777	28.8043	39.6039
Pseudo second-order					
q _e , exp (mg g ⁻¹)	4.9859	24.1981	43.8152	61.684	81.77
q _e , cal (mg g ⁻¹)	5.005	24.6305	42.5532	61.728	83.333
R ²	0.9986	0.9833	0.9992	0.9996	0.9989
HYBRID	7.317 × 10 ⁻⁵	0.00773	0.03635	3.1 × 10 ⁻⁵	0.02988
MPSD	1.468 × 10 ⁻⁵	0.000319	0.00083	5.09 × 10 ⁻⁷	0.000365
ARE	- 0.003830	- 0.01787	0.028803	- 0.00071	- 0.01911
Δq	0.09577	0.446729	0.72007	0.017833	0.477865
S _{RE}	0.007634	0.2073	0.6166	0.02164	0.7719
Elovich					
q _e ,exp (mg g ⁻¹)	4.9859	24.1981	43.8152	61.684	81.77
q _e , cal (mg g ⁻¹)	4.9889	23.6859	42.7181	61.4962	82.3027
R ²	0.4294	0.0791	0.8596	0.9643	0.7837
HYBRID	1.8051 × 10 ⁻⁶	0.01084	0.02747	0.00057	0.00347
MPSD	3.6204 × 10 ⁻⁷	0.000448	0.000627	9.27 × 10 ⁻⁶	4.24 × 10 ⁻⁵
ARE	- 0.0006017	0.021167	0.025039	0.003045	- 0.00651
Δq	0.015042	0.529174	0.625981	0.076114	0.162865
S _{RE}	0.001199	0.24556	0.53603	0.09237	0.2631
Avrami					
q _e ,exp (mg g ⁻¹)	4.9859	24.1981	43.8152	61.684	81.77
q _e , cal (mg g ⁻¹)	4.873	17.5472	41.307	60.1006	78.3886
R ²	0.4294	0.0791	0.8596	0.9643	0.7837
HYBRID	0.002556	1.8280	0.1436	0.04065	0.1398
MPSD	0.0005127	0.07554	0.003277	0.000659	0.00171
ARE	0.02264	0.2748	0.05724	0.02567	0.04135
Δq	0.5661	6.8713	1.4311	0.6417	1.0338
S _{RE}	0.04512	3.1880	1.2255	0.7789	1.6700
Power function (fractional power)					
q _e ,exp (mg g ⁻¹)	4.9859	24.1981	43.8152	61.684	81.77
q _e , cal (mg g ⁻¹)	4.9906	23.6629	42.7202	61.5025	82.2843
R ²	0.5443	0.5827	0.7156	0.6609	0.6989
HYBRID	4.43 × 10 ⁻⁶	0.01184	0.02737	0.00053	0.00323
MPSD	8.886 × 10 ⁻⁷	0.000489	0.000625	8.66 × 10 ⁻⁶	3.96 × 10 ⁻⁵
ARE	- 0.000943	0.022117	0.024991	0.002942	- 0.00629
Δq	0.0236	0.5529	0.6247	0.07356	0.15724
S _{RE}	0.001878	0.2565	0.535004	0.089279	0.254005

Table 7. Statistical Error validity data on kinetics models of adsorption of Cu(II) onto nZVI.

is routed by ion exchange. Ion-exchange, electrostatic and physiochemical mechanistic nature of the adsorption supported by the previous studies^{50,58,59}.

Conclusion

This study revealed the effectiveness of nZVI as an auspicious nano sorbent for the efficient elimination of endocrine disruptive heavy metal ions. The quality physicochemical properties of nZVI gave it an edge among the list of other nano-adsorbents compared. Evidence of the adsorption of Cu²⁺ onto nZVI was revealed by a change in morphology and elemental distribution by SEM and EDX respectively from post adsorption characterization.

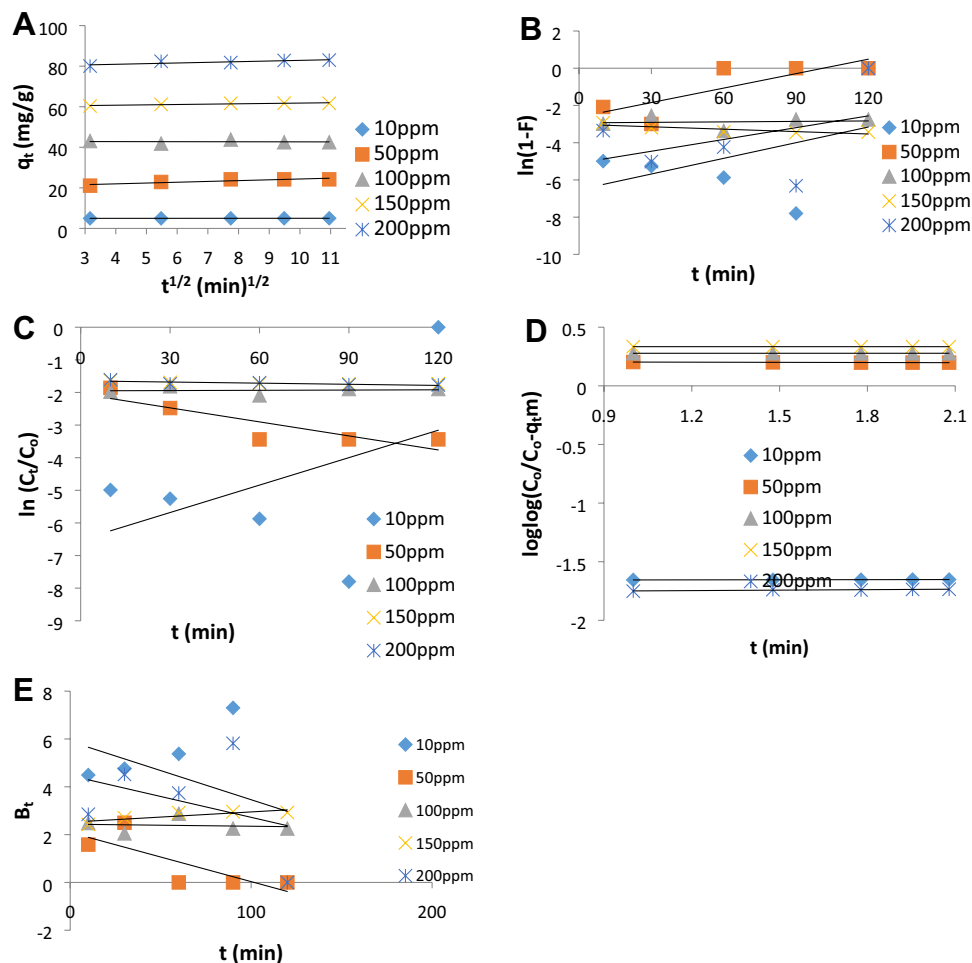


Figure 3. Linearized plots of (A) intraparticle diffusion, (B) liquid film diffusivity, (C) external diffusion, (D) Bangham and (E) Boyd models for adsorption of Cu²⁺ onto nZVI at 10 ppm, 50 ppm, 100 ppm, 150 ppm and 200 ppm.

Adsorption mechanism models	Cu ²⁺ concentration				
	10 ppm	50 ppm	100 ppm	150 ppm	200 ppm
Intraparticle diffusion					
k_{ip} (mg g ⁻¹ min ^{-0.5})	0.0047	0.3993	- 0.0199	0.1743	0.3224
C	4.9501	20.378	42.883	60.052	79.634
R ²	0.9795	0.8321	0.0069	0.8322	0.7185
Liquid film diffusion					
K_{LFD}	- 0.0281	- 0.0259	- 0.0009	0.0043	- 0.0211
C	- 6.5233	- 2.6199	- 2.9337	- 3.0157	- 5.0927
R ²	0.1855	0.6484	0.0147	0.7275	1.552
External diffusion					
k_{ext}	- 0.0281	0.0143	0.0003	0.0008	0.0012
C	- 6.5233	- 2.0416	- 0.0119	- 1.6533	- 1.6452
R ²	0.1855	0.7597	0.0119	0.7058	0.6417
Bangham					
\bar{a}	0.003	- 0.0047	0.0004	0.00008	0.0133
Ko	0.025285	1.8564	2.1820	2.4858	0.019896
R ²	0.9404	0.9344	0.0078	0.9351	0.7968
Boyd					
R ²	0.1623	0.6170	0.0147	0.7275	0.1258

Table 8. Adsorption Mechanism models for Sorption of Cu²⁺ onto nZVI.

T(K)	ΔG (kJ mol ⁻¹)	ΔH (kJ mol ⁻¹)	ΔS (J mol ⁻¹ K ⁻¹)	Kc
298	-1.6765	+50.6059	174.679	1.96711
308	-2.8163			3.00304
318	-4.4575			5.39623
328	-7.7182			16.9419
338	-7.9602			16.9825

Table 9. Thermodynamic parameters for adsorption of Cu²⁺ onto nZVI.

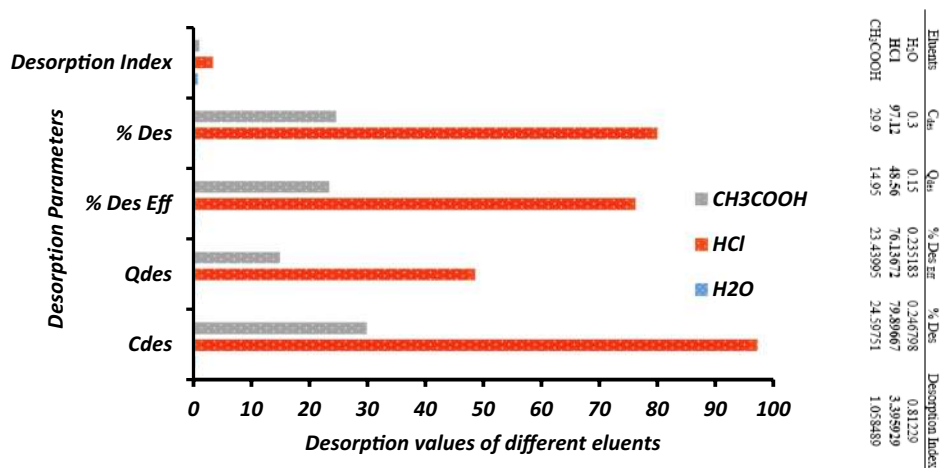


Figure 4. Comparative effect of different eluents in the desorption of Cu²⁺ from Cu²⁺-loaded nZVI.

The adsorption of Cu²⁺ onto nZVI was well influenced by operational parameters. Optimum adsorption was achieved at pH 6 with 98.31% removal efficiency, 73.73 mg g⁻¹ quantity adsorbed and 200 rpm stirring speed. Thermodynamics parameters ΔH° (+50.6059 kJ mol⁻¹), ΔS° (174.6790 J mol⁻¹ K⁻¹), ΔG° (-1.6765 kJ mol⁻¹ to -7.9602 kJ mol⁻¹). Indicated random, feasible, spontaneous, and endothermic nature of the adsorption process. The adsorption behavior was well explained by the Langmuir isotherm model and it followed the following order: Langmuir > Jossen/Elovich > Freundlich/Halsey > Temkin > Fowler–Guggenheim > Redlich–Peterson > DKR > Flory–Huggins > Kiselev > Harkin–Jura > Jovanovic. Langmuir best described equilibrium data. The Langmuir monolayer adsorption capacity (90.09 mg g⁻¹) surpassed other nano-adsorbents utilized for the adsorption of Cu(II) ion. The Pseudo-second-order (PSO) best described the kinetics model based on R² values greater than 0.99, close agreement between q_e, exp and q_e, cal and lower values of the five rigorous statistical validity models (Δq_t , ARE, HYBRD, MPSD, and S_{RE}). The mechanism model was pore diffusion dependent. Best desorption capacity and the index was portrayed by HCl indicating that ion-exchange, electrostatic, and physisorption mechanism. Based on the capacity displayed by nZVI in adsorption of EDC Cu²⁺, it could be recommended for effective industrial treatment of heavy metal ions.

Data availability

Available data are presented in the study and no other data were used to support the study.

Received: 24 April 2021; Accepted: 6 July 2021

Published online: 12 August 2021

References

1. Tapia-Orozco, N. *et al.* Removal strategies for endocrine-disrupting chemicals using cellulose-based materials as adsorbents: A review. *J. Environ. Chem. Eng.* **4**, 3122–3142 (2016).
2. Handy, R. D. Chronic effects of copper exposure versus endocrine toxicity: Two sides of the same toxicological process?. *Comp. Biochem. Physiol. A Mol. Integr. Physiol.* **135**, 25–38 (2003).
3. Saravanan, A. *et al.* Simultaneous removal of Cu(II) and reactive green 6 dye from wastewater using immobilized mixed fungal biomass and its recovery. *Chemosphere* **271**, 129519 (2021).
4. Saravanan, A., Senthil Kumar, P. & Mugilan, R. Ultrasonic-assisted activated biomass (fishtail palm *Caryota urens* seeds) for the sequestration of copper ions from wastewater. *Res. Chem. Intermed.* **42**, 3117–3146 (2016).
5. Dada, A. O., Latona, D. F., Ojediran, O. J. & Nath, O. O. Adsorption of Cu (II) onto bamboo supported manganese (BS-Mn) nanocomposite: Effect of operational parameters, kinetic, isotherms, and thermodynamic studies. *J. Appl. Sci. Environ. Manag.* **20**, 409–422 (2016).
6. Dada, A. O., Adekola, F. A. & Odeunmi, E. O. Kinetics, mechanism, isotherm and thermodynamic studies of liquid-phase adsorption of Pb²⁺ onto wood activated carbon-supported zerovalent iron (WAC-ZVI) nanocomposite. *Cogent Chem.* **68**, 1351653 (2017).

7. Saravanan, A. *et al.* Effective adsorption of Cu(II) ions on sustainable adsorbent derived from mixed biomass (*Aspergillus campestris* and agro-waste): Optimization, isotherm and kinetics study. *Groundw. Sustain. Dev.* **11**, 100460 (2020).
8. Das, S., Sen, B. & Debnath, N. Recent trends in nanomaterials applications in environmental monitoring and remediation. *Environ. Sci. Pollut. Res.* **22**, 18333–18344 (2015).
9. Sivaranjane, R. & Kumar, P. S. A review on cleaner approach for effective separation of toxic pollutants from wastewater using carbon Sphere's as adsorbent: Preparation, activation, and applications. *J. Clean. Prod.* **291**, 125911 (2021).
10. Keane, E. & Di Giulio, D. R. Fate, transport, and toxicity of nanoscale zero-valent iron (nZVI) used during superfund remediation. *Nicholas Sch. Environ.* **52** (2009). https://dukespace.lib.duke.edu/dspace/bitstream/handle/10161/2172/Keane_MP_042610.pdf?sequence=1.
11. Mukherjee, R., Kumar, R., Sinha, A., Lama, Y. & Saha, A. K. A review on synthesis, characterization, and applications of nano zero valent iron (nZVI) for environmental remediation. *Crit. Rev. Environ. Sci. Technol.* **46**, 443–466 (2016).
12. Singh, R., Misra, V. & Singh, R. P. Removal of hexavalent chromium from contaminated groundwater using zero-valent iron nanoparticles. *Environ. Monit. Assess* **184**, 3643–3651 (2012).
13. Saravanan, A. *et al.* Phytoremediation of Cr(VI) ion contaminated soil using Black gram (*Vigna mungo*): Assessment of removal capacity. *J. Environ. Chem. Eng.* **7**, 103052 (2019).
14. Ahmad, M. A., Ahmad Puad, N. A. & Bello, O. S. Kinetic, equilibrium and thermodynamic studies of synthetic dye removal using pomegranate peel activated carbon prepared by microwave-induced KOH activation. *Water Resour. Ind.* **6**, 18–35 (2014).
15. Gong, J. *et al.* Shellac-coated iron oxide nanoparticles for removal of cadmium(II) ions from aqueous solution. *J. Environ. Sci. (China)* **24**, 1165–1173 (2012).
16. Prabu, D., Parthiban, R., Senthil Kumar, P., Kumari, N. & Saikia, P. Adsorption of copper ions onto nano-scale zero-valent iron impregnated cashew nutshell. *Desalin. Water Treat.* **57**, 6487–6502 (2016).
17. Dada, O. A., Adekola, F. A. & Odeunmi, E. O. Kinetics and equilibrium models for sorption of Cu(II) onto a novel manganese nano-adsorbent. *J. Dispers. Sci. Technol.* **37**, 119–133 (2016).
18. Mtshatsheni, K. N. G., Ofomaja, A. E. & Naidoo, E. B. Synthesis and optimization of reaction variables in the preparation of pine-magnetite composite for removal of methylene blue dye. *S. Afr. J. Chem. Eng.* **29**, 33–41 (2019).
19. Dada, A. O. *et al.* Kinetics and thermodynamics of adsorption of rhodamine B onto bentonite supported nanoscale zerovalent iron nanocomposite. *J. Phys. Conf. Ser.* **1299**, 012106 (2019).
20. Bello, O. S. *et al.* Rhodamine B dye sequestration using *Gmelina aborea* leaf powder. *Heliyon* **6**, e02872 (2020).
21. Bhatti, H. N., Jabeen, A., Iqbal, M., Noreen, S. & Naseem, Z. Adsorptive behavior of rice bran-based composites for malachite green dye: Isotherm, kinetic and thermodynamic studies. *J. Mol. Liq.* **237**, 322–333 (2017).
22. Olalekan, A. P., Dada, A. O. & Adesina, O. A. Review: Silica aerogel as a viable adsorbent for oil spill remediation. *J. Encapsul. Adsorpt. Sci.* <https://doi.org/10.4236/jeas.2014.44013> (2014).
23. Heidari-Chaleshtori, M. & Nezamzadeh-Ejhi, A. Clinoptilolite nano-particles modified with aspartic acid for removal of Cu(II) from aqueous solutions: Isotherms and kinetic aspects. *New J. Chem.* **39**, 9396–9406 (2015).
24. Dada, A. O., Adekola, F. A. & Odeunmi, E. O. Liquid phase scavenging of Cd (II) and Cu (II) ions onto novel nanoscale zerovalent manganese (nZVMn): Equilibrium, kinetic and thermodynamic studies. *Environ. Nanotechnol. Monit. Manag.* **8**, 63–72 (2017).
25. Dada, A. O., Adekola, F. A. & Odeunmi, E. O. A novel zerovalent manganese for removal of copper ions: Synthesis, characterization and adsorption studies. *Appl. Water Sci.* <https://doi.org/10.1007/s13201-015-0360-5> (2015).
26. Nguéagni, P. T. *et al.* Adsorption of Cu(II) ions by modified horn core: Effect of temperature on adsorbent preparation and extended application in river water. *J. Mol. Liq.* **298**, 112023 (2020).
27. Rajabi, M. *et al.* Adsorption of malachite green from aqueous solution by carboxylate group functionalized multi-walled carbon nanotubes: Determination of equilibrium and kinetics parameters. *J. Ind. Eng. Chem.* **34**, 130–138 (2016).
28. Adekola, F. A., Hodonou, D. S. S. & Adegoke, H. I. Thermodynamic and kinetic studies of biosorption of iron and manganese from aqueous medium using rice husk ash. *Appl. Water Sci.* **6**, 319–330 (2016).
29. Guan, H. *et al.* A facile method to synthesize magnetic nanoparticles chelated with copper(II) for selective adsorption of bovine hemoglobin. *Korean J. Chem. Eng.* **37**, 1097–1106 (2020).
30. Şentürk, İ & Yıldız, M. R. Highly efficient removal from aqueous solution by adsorption of Maxilon Red GRL dye using activated pine sawdust. *Korean J. Chem. Eng.* **37**, 985–999 (2020).
31. Liu, Z., Li, X., Zhan, P., Hu, F. & Ye, X. Removal of cadmium and copper from water by a magnetic adsorbent of PFM: Adsorption performance and micro-structural morphology. *Sep. Purif. Technol.* **206**, 199–207 (2018).
32. Baby, R., Saifullah, B. & Hussein, M. Z. Palm Kernel Shell as an effective adsorbent for the treatment of heavy metal contaminated water. *Sci. Rep.* **9**, 1–11 (2019).
33. Medhi, H. & Bhattacharyya, K. G. Kinetic and mechanistic studies on adsorption of Cu(II) in aqueous medium onto montmorillonite K10 and its modified derivative. *New J. Chem.* **41**, 13533–13552 (2017).
34. Liu, G., Ma, J., Li, X. & Qin, Q. Adsorption of bisphenol A from aqueous solution onto activated carbons with different modification treatments. *J. Hazard. Mater.* **164**, 1275–1280 (2009).
35. Kampalanonwat, P. & Supaphol, P. The study of competitive adsorption of heavy metal ions from aqueous solution by aminated polyacrylonitrile nanofiber mats. *Energy Proc.* **56**, 142–151 (2014).
36. Del Bubba, M. *et al.* Physicochemical properties and sorption capacities of sawdust-based biochars and commercial activated carbons towards ethoxylated alkylphenols and their phenolic metabolites in effluent wastewater from a textile district. *Sci. Total Environ.* **708**, 135217 (2020).
37. Dahri, M. K., Kooh, M. R. R. & Lim, L. B. L. Water remediation using low-cost adsorbent walnut shell for removal of malachite green: Equilibrium, kinetics, thermodynamic and regeneration studies. *J. Environ. Chem. Eng.* **2**, 1434–1444 (2014).
38. Zhao, Y. *et al.* Adsorptive removal of endocrine-disrupting compounds and a pharmaceutical using activated charcoal from aqueous solution: Kinetics, equilibrium, and mechanism studies. *Environ. Sci. Pollut. Res.* **26**, 33897–33905 (2019).
39. Song, C. *et al.* Adsorption studies of coconut shell carbons prepared by KOH activation for removal of lead(II) from aqueous solutions. *Sustainability* **6**, 86–98. <https://doi.org/10.3390/su6010086> (2014).
40. Rangabhashiyam, S., Anu, N., Giri Nandagopal, M. S. & Selvaraju, N. Relevance of isotherm models in biosorption of pollutants by agricultural byproducts. *J. Environ. Chem. Eng.* **2**, 398–414 (2014).
41. Dada, A. O. *et al.* Article ID: IJCIET_09_13_159 Adsorption of rhodamine B dye onto chitosan supported zerovalent iron nanocomposite (C-nZVI). *Int. J. Civ. Eng. Technol.* **9**, 1591–1605 (2018).
42. Hamdaoui, O. & Naffrechoux, E. Modeling of adsorption isotherms of phenol and chlorophenols onto granular activated carbon. Part I. Two-parameter models and equations allowing determination of thermodynamic parameters. *J. Hazard. Mater.* **147**, 381–394 (2007).
43. Ayawei, N., Ebelegi, A. N. & Wankasi, D. Modelling and interpretation of adsorption isotherms. *J. Chem.* **2017**, 1–11 (2017).
44. Al-Ghouti, M. A. & Da'ana, D. A. Guidelines for the use and interpretation of adsorption isotherm models: A review. *J. Hazard. Mater.* **393**, 122383 (2020).
45. Rangabhashiyam, S. & Balasubramanian, P. Performance of novel biosorbents prepared using native and NaOH treated *Peltophorum pterocarpum* fruit shells for the removal of malachite green. *Bioresour. Technol. Rep.* **3**, 75–81 (2018).

46. Dada, A. O. Modeling of biosorption of Pb (II) and Zn (II) ions onto PAMRH: Langmuir, Freundlich, Temkin, Dubinin–Raduskevich, Jovanovic, Flory–Huggins, Fowler–Guggenheim and Kiselev comparative isotherm studies. *Int. J. Mech. Eng. Technol. (IJMET)* **10**, 1048–1058 (2019).
47. Dada, A. O. *et al.* For biosorption of indigo carmine dye: Kinetics, isotherm, and thermodynamic studies. *Int. J. Phytoremediat.* **1–14** (2020).
48. Sivarajasekar, N. & Baskar, R. Adsorption of basic red 9 onto activated carbon derived from immature cotton seeds: Isotherm studies and error analysis. *Desalin. Water Treat.* **52**, 7743–7765 (2014).
49. Abdul, J. M., Vigneswaran, S., Shim, W. G. & Kandasamy, J. Removal of metsulfuron methyl by granular activated carbon adsorption. *Desalin. Water Treat.* **21**, 247–254 (2010).
50. Hemavathy, R. R. V., Kumar, P. S., Suganya, S., Swetha, V. & Varjani, S. J. Modelling on the removal of toxic metal ions from aquatic system by different surface modified *Cassia fistula* seeds. *Bioresour. Technol.* **281**, 1–9 (2019).
51. Boparai, H. K., Joseph, M. & O’Carroll, D. M. Kinetics and thermodynamics of cadmium ion removal by adsorption onto nano zerovalent iron particles. *J. Hazard. Mater.* **186**, 458–465 (2011).
52. Suganya, S. An investigation of adsorption parameters on ZVI-AC nanocomposite in the displacement of Se(IV) ions through CCD analysis. *J. Ind. Eng. Chem.* **75**, 211–223 (2019).
53. Azmier, M. & Norhidayah, A. Modified durian seed as adsorbent for the removal of methyl red dye from aqueous solutions. *Appl. Water. Sci.* <https://doi.org/10.1007/s13201-014-0208-4> (2014).
54. Senthil Kumar, P., Senthamarai, C., Sai Deepthi, A. S. L. & Bharani, R. Adsorption isotherms, kinetics and mechanism of Pb(II) ions removal from aqueous solution using chemically modified agricultural waste. *Can. J. Chem. Eng.* **91**, 1950–1956 (2013).
55. Hao, Y. M., Man, C. & Hu, Z. B. Effective removal of Cu (II) ions from aqueous solution by amino-functionalized magnetic nanoparticles. *J. Hazard. Mater.* **184**, 392–399 (2010).
56. Kaveeshwar, A. R. *et al.* Adsorption properties and mechanism of barium (II) and strontium (II) removal from fracking wastewater using pecan shell based activated carbon. *J. Clean. Prod.* **193**, 1–13 (2018).
57. Lezczano, J. M. *et al.* Sorption and desorption of Cd, Cu and Pb using biomass from an eutrophized habitat in monometallic and bimetallic systems. *J. Environ. Manag.* **92**, 2666–2674 (2011).
58. Petrović, M. *et al.* Mechanism of adsorption of Cu²⁺ and Zn²⁺ on the corn silk (*Zea mays* L.). *Ecol. Eng.* **99**, 83–90 (2017).
59. Türkmen, D., Yilmaz, E., Öztürk, N., Akgöl, S. & Denizli, A. Poly(hydroxyethyl methacrylate) nanobeads containing imidazole groups for removal of Cu(II) ions. *Mater. Sci. Eng. C* **29**, 2072–2078 (2009).

Acknowledgements

The research enabling environment provided by the Management of Landmark University is appreciated. The assistance rendered by Dr. Ogunlaja Adeniyi in Rhodes University, South Africa for morphology characterization is thankfully acknowledged.

Author contributions

A.O.D., FA.A., E.O.O., A.S.O. carried out the experiments, analyzed the results for the adsorption’ data. A.O.D., FA.A., E.O.O., O.S.B. fitted the thermodynamics and kinetics of adsorption curves. A.O.D., FA.A., and E.O.O., drafted the manuscript. All authors reviewed and approved the manuscript.

Competing interests

The authors declare no competing interests.


Additional information

Supplementary Information The online version contains supplementary material available at <https://doi.org/10.1038/s41598-021-95090-8>.

Correspondence and requests for materials should be addressed to A.O.D.

Reprints and permissions information is available at www.nature.com/reprints.

Publisher’s note Springer Nature remains neutral with regard to jurisdictional claims in published maps and institutional affiliations.

 **Open Access** This article is licensed under a Creative Commons Attribution 4.0 International License, which permits use, sharing, adaptation, distribution and reproduction in any medium or format, as long as you give appropriate credit to the original author(s) and the source, provide a link to the Creative Commons licence, and indicate if changes were made. The images or other third party material in this article are included in the article’s Creative Commons licence, unless indicated otherwise in a credit line to the material. If material is not included in the article’s Creative Commons licence and your intended use is not permitted by statutory regulation or exceeds the permitted use, you will need to obtain permission directly from the copyright holder. To view a copy of this licence, visit <http://creativecommons.org/licenses/by/4.0/>.

© The Author(s) 2021